International Journal of Nanomedicine

Dovepress
open access to scientific and medical research

Open Access Full Text Article

ORIGINAL RESEARCH

Multifunctional Lithium-Doped Mesoporous Nanoparticles for Effective Dentin Regeneration in vivo

Zitian Liang[1,*], Ding Chen[2,*], Ye Jiang[1], Zhikang Su[2], Yixing Pi[2], Tao Luo[2], Qianzhou Jiang[1], Li Yang[1], Lvhua Guo[2]

[1]Department of Endodontics, Affiliated Stomatology Hospital of Guangzhou Medical University, Guangdong Engineering Research Center of Oral Restoration and Reconstruction, Guangzhou Key Laboratory of Basic and Applied Research of Oral Regenerative Medicine, Guangzhou, Guangdong, 510182, People's Republic of China; [2]Department of Prosthodontics, Affiliated Stomatology Hospital of Guangzhou Medical University, Guangdong Engineering Research Center of Oral Restoration and Reconstruction, Guangzhou Key Laboratory of Basic and Applied Research of Oral Regenerative Medicine, Guangzhou, Guangdong, 510182, People's Republic of China

*These authors contributed equally to this work

Correspondence: Li Yang; Lvhua Guo, Affiliated Stomatology Hospital of Guangzhou Medical University, No. 195 West Dongfeng Road, Guangzhou, 510182, People's Republic of China, Tel +86-020-81299942, Email 2019686001@gzhmu.edu.cn; 2010686002@gzhmu.edu.cn

Introduction: Effective infection control without irritating the pulp tissue is the key to successful vital pulp therapy. Developing a novel antibacterial biomaterial that promotes dentin regeneration for pulp capping is thus a promising strategy for enhancing vital pulp therapy.

Methods: Lithium-doped mesoporous nanoparticles (Li-MNPs) were synthesized using an alkali-catalyzed sol-gel method. The particle size, elemental distribution, surface morphology, pore structure, and ion release from Li-MNPs were measured. Human dental pulp stem cells (hDPSCs) and *Streptococcus mutans* (*S. mutans*) were used to evaluate the biological effects of Li-MNPs. In addition, a dental pulp exposure mouse model was used to evaluate the regenerative effects of Li-MNPs.

Results: Li-MNPs had a larger surface area (221.18 m^2/g), a larger pore volume (0.25 cm^3/g), and a smaller particle size (520.92 ± 35.21 nm) than MNPs. The in vitro investigation demonstrated that Li-MNPs greatly enhanced the biomineralization and odontogenic differentiation of hDPSCs through the Wnt/β-catenin signaling pathway. Li-MNPs showed a strong antibacterial effect on *S. mutans*. As expected, Li-MNPs significantly promoted dentin regeneration in situ and in vivo.

Conclusion: Li-MNPs promoted dentin regeneration and inhibited *S. mutans* growth, implying a possible application as a pulp capping agent in vital pulp therapy.

Keywords: lithium, mesoporous nanoparticles, dental pulp stem cells, dentin regeneration, Wnt/β-catenin signaling pathway, antibacterial properties

Introduction

The preservation of vital pulp plays a significant role in prolonging the period of permanent teeth's normal function. On the one hand, it enables the continuous development of young permanent teeth;[1] on the other hand, dental pulp, as a biological receptor, responds defensively to pathological stimuli and forms tertiary dentin to prevent the further development of lesions.[2] Pulp capping is a dental procedure that attempts to preserve vital pulp by placing dental materials directly onto the vital pulp tissues of affected teeth.[3] Therefore, an ideal pulp capping agent requires anti-infective, antibacterial, and pro-dentin regenerative properties.

It has been over 90 years since Hermann first used calcium hydroxide in the 1920s to treat endodontics.[4] Calcium hydroxide raises the pH of the microenvironment, creating an alkaline environment for sterilization of the pulp tissue, causing necrosis of the exposed pulp and an inflammatory response that may result in tertiary dentin formation.[5] Due to

Received: 27 June 2023
Accepted: 7 September 2023
Published: 18 September 2023

Graphical Abstract

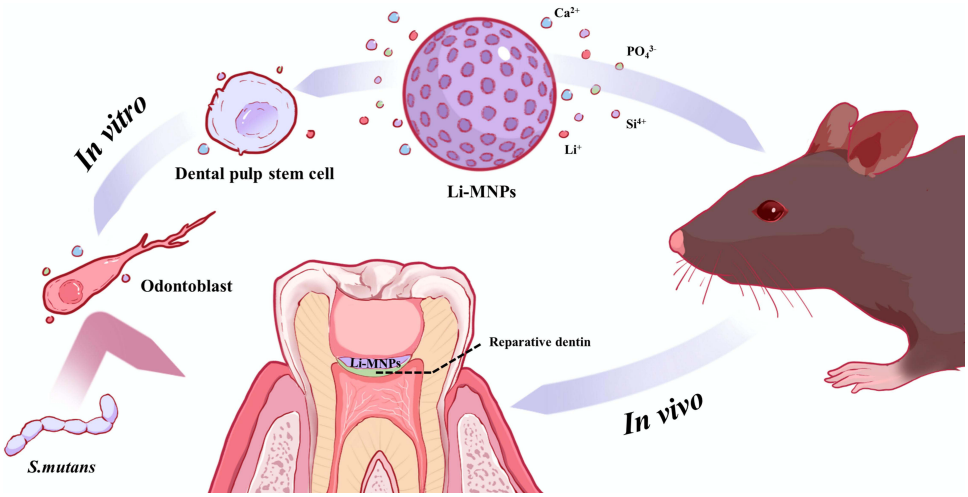

the poor long-term clinical success of calcium hydroxide,[6,7] mineral trioxide aggregate (MTA) has attracted the attention of clinicians and has become the gold standard among pulp capping agents because of its excellent biocompatibility.[8] MTA has been proven to promote pulp tissue regeneration and has good clinical efficacy; however, it also has some disadvantages, such as its long curing time, an inability to bind dentin, and that it contains bismuth trioxide, iron, and magnesium elements, which tend to discolor the crown, etc.[9,10] Furthermore, the antibacterial activity of MTA against *S. mutans*, the key causative agent of caries, is controversial.[11–15]

MNPs (e.g, bioactive glass-based MNPs, silica MNPs, hydroxyapatite MNPs) possess high surface areas and highly organized mesoporous channel structures, which have great potential for application in drug delivery and tissue regeneration.[16–18] Bioactive glass-based MNPs possess excellent biological activity and display promising characteristics in facilitating the localized delivery of therapeutically active ions (eg, lithium, zinc, strontium, or copper) to enhance their biological properties.[19–21] Among them, lithium has a long history as a canonical Wnt signaling pathway activator, capable of effectively blocking GSK3β activity and leading to the stability of free cytosolic β-catenin, resulting in increased intracellular Wnt activity.[22–24] In a study by Ali et al, it was revealed that surface pre-reacted glass fillers infused with lithium demonstrated a capacity to incite odontogenic differentiation in hDPSCs. Furthermore, these fillers exhibited the ability to promote dentin formation within a rat pulp capping model through the Wnt/β-catenin signaling pathway.[25] In addition, lithium has garnered attention for its notable antibacterial properties and its lack of susceptibility to bacterial resistance, which are required for pulp capping agents to combat infections in the pulp tissue.[26] It is possible that lithium-doped bioactive glass-based MNPs (Li-MNPs) could serve as a bioactive pulp capping agent that is both antibacterial and effective in stimulating dentin regeneration.

To test this hypothesis, this study aimed to synthesize Li-MNPs based on bioactive glass composition, evaluate their effect on dentin regeneration, and test their ability to inhibit the growth of *S. mutans*.

Materials and Methods

Synthesis of Lithium-Doped Mesoporous Nanoparticles (Li-MNPs)

Lithium-free and lithium-doped mesoporous nanoparticles, namely, MNPs and Li-MNPs, respectively, based on bioactive glass compositions of 60 SiO_2 - (36-x) CaO - x Li_2O - 4 P_2O_5 (x=0 and 5 mol%), were synthesized using an alkali-catalyzed sol-gel approach with dodecylamine (DDA) as the catalyst agent and cetyltrimethylammonium bromide (CTAB) as a structural template agent.[27] The exact amounts of material used in the synthesis process are shown in Table 1. Briefly, DDA (Aladdin, China) was dissolved into a mixture of ethanol (Damao, China) and ultrapure deionized

Table 1 The Exact Amounts of Material Used in the Synthesis Process

Sample	Ethanol (mL)	DW (mL)	DDA (g)	CTAB (g)	TEOS (mL)	TEP (mL)	CN (g)	LN (g)
MNPs	80	20	4	0.07	2.23	0.23	1.417	0
Li-MNPs	80	20	4	0.07	2.23	0.23	1.215	0.114

water (DW) (18.2 MΩ, HealForce ultrapure water system, China) under vigorous stirring for 10 min. Then CTAB (Macklin, China) was dissolved into the resultant solution, followed by stirring for 30 min. Tetraethyl orthosilicate (TEOS) (Sigma-Aldrich, USA), triethyl phosphate (TEP) (Sigma-Aldrich, USA), and calcium nitrate tetrahydrate (CN) (Damao, China) or lithium nitrate hydrate (LN) (Macklin, China) were dissolved in sequence at intervals of 30 min while stirring at 40 °C. The resulting mixture was continuously stirred for 6 h to attain a white precipitate, followed by centrifuging, alternately washing three times with ethanol and DW, and drying at 60 °C for 24 h to attain dry powers. The samples were sintered in air at 650 °C for 3 h to attain the final products.

The Examination of Li-MNPs Using Different Technologies

The synthesized Li-MNPs were characterized using time of flight secondary ion mass spectrometry (TOF-SIMS) (PHI nanoTOF II Time-of-Flight SIMS, Japan), scanning electron microscopy (SEM) (Zeiss Sigma 300, Germany), transmission electron microscopy (TEM) (FEI Tecnai G2 f20s-twin, USA), nitrogen (N_2) adsorption–desorption isotherms (Micromeritics ASAP 2020, USA), X-ray diffraction (XRD) (Rigaku UltimaIV, Japan), Fourier transform infrared spectroscopy (FT-IR) (Bruker TENSOR 27, Germany), and a Zetasizer Nanoseries (Malvern Zetasizer Nano ZS90, England). The particle size analyses of the SEM photographs of MNPs and Li-MNPs were performed using the Nano Measurer software (Fudan University, China). The Brunauer–Emmett–Teller (BET) and Barrett–Joyner–Halenda (BJH) approaches were used to evaluate the specific surface area, pore volume, and pore size distribution.

In vitro Ion Release

Ion release was measured using an inductively coupled plasma-optical emission spectrometer (ICP-OES) (Agilent 720, USA) to evaluate the concentrations of silicon (Si), calcium (Ca), phosphorus (P), and lithium (Li) ions in the soaking solution. Briefly, 20 mg of MNPs or Li-MNPs were immersed in 20 mL of Tris-HCl (0.05 M, pH=7.4, Yuanye, China) and shaken at 120 rpm for up to 28 days at 37°C. The extract was collected and used for ion release measurements at specified time points (1, 3, 5, 7, 14, and 28 days).

Cell Culture and Identification

The hDPSCs used in the current study were obtained from Procell Life Science & Technology (Wuhan, China). Cells between passages two and five were used throughout the experiments. The cells were cultured at 37 °C in 5% CO_2 with a culture medium (CM) which comprised α-MEM (Gibco, USA), fetal bovine serum (10%, Gibco, USA), and penicillin/streptomycin (1%, Gibco, USA). The medium changed every three days. The cells were cultured in an odontogenic supplemental medium (OM) containing β-glycerophosphate (10 mM), ascorbic acid (50 μg/mL), dexamethasone (10 nM) and the abovementioned CM to induce the odontogenesis of hDPSCs.[28] Cells between passages two and three were selected, and positive [CD29, CD44, CD73, CD90, CD105; (Biolegend, USA)] and negative antibodies [CD11b, CD19, CD34, CD45, HLA-DR; (Biolegend, USA)] were detected using flow cytometry (BD, USA). Analysis was performed using Flowjo software (BD, USA). The positive antibody CD90 (Boster, China) was detected using immunofluorescence.

Preparation of Extracts

The extracts were obtained based on the approaches of the International Standard Organization (ISO 10993–5). Briefly, 2 g of MNPs or Li-MNPs were soaked in 10 mL of α-MEM, and the mixture was shaken at 120 rpm for 24 h at 37 °C. Then, the extracts were centrifuged at 4000 rpm for 15 min and sterilized by filtration through a 0.22 μm filter (Millipore, USA). The extract-configured culture/odontogenic supplemental medium (eCM/eOM) was formed by replacing the α-

MEM in CM or OM by diluting the extract at different concentrations (1/2, 1/4, 1/8, 1/16, 1/32, 1/64, and 1/128) and replacing it in equal amounts.

Cell Proliferation Assay

The measurement of hDPSC proliferation in response to the MNP and Li-MNP extracts was conducted using a Cell Counting Kit-8 assay (CCK-8) (Dojindo, Japan). Briefly, the seeding of the cells into 96-well plates was conducted at a density of 2×10^3 cells/well, followed by treatment with various concentrations of MNP and Li-MNP eCM (1/2, 1/4, 1/8, 1/16, 1/32, 1/64 and 1/128). After which the culturing lasted for 1, 3, 5, and 7 days; the medium was modified with CCK-8 solution (10 μL/well) and CM (90 μL/well), then kept away from light in an incubator at 37 °C for 2 h. The absorbance was recorded at 450 nm using an ELX Ultra microplate reader (BioTek, USA), and the optical density (OD) was measured for cell viability (n=6).

Alkaline Phosphatase (ALP) Staining and Quantification

The cultivation of hDPSCs was carried out at 3×10^4 cells/well in 48-well plates, which were then treated with various concentrations of MNP or Li-MNP eOM (1/8, 1/16, 1/32, 1/64, and 1/128) for 7 days, with the medium changed every 3 days. For ALP staining: The cells were fixed with 4% PFA (Biosharp, China), followed by washing with phosphate-buffered saline (PBS) (Gibco, USA) and assessing with a BCIP/NBT ALP color development kit (Beyotime, China). For ALP quantification: The cells were lysed for protein extraction in cell lysis buffer for Western blotting and immunoprecipitation (IP) without inhibitors (Beyotime, China) and evaluated using an ALP assay kit (Beyotime, China) based on the manufacturer's instructions.

Alizarin Red Staining (ARS)

The seeding of hDPSCs was performed at 1.5×10^5 cells/well in 6-well plates. When confluence was reached, the medium was replaced with OM, 1/32 MNPs, eOM, and 1/32 Li-MNPs eOM. Three weeks later, the cells were fixed with 4% PFA and stained using Alizarin red S solution (1%, pH 4.2, Solarbio, China).

Real-Time Quantitative Polymerase Chain Reaction (RT-qPCR)

The hDPSCs were cultured with OM, 1/32 MNPs eOM, and 1/32 Li-MNPs eOM in each of the 6-well plates for certain time points. The extraction of total RNA was performed using an EZ-press RNA purification kit (EZBioscience, USA) based on the manufacturer's instructions. The RNA (500 ng) was reverse-transcribed to cDNA according to the method described elsewhere.[29] Glyceraldehyde-3-phosphate dehydrogenase (GAPDH) was employed as the internal control. All primer sequences are presented in Table 2. The conditions for RT-qPCR were set as follows: denaturation at 95°C (30 s), 40 cycles at 95°C (5 s), and 60 °C (30 s, annealing), which was followed by a final dissociation step. The RT-qPCR reactions were carried out using an SYBR Green pro taq HS premix (Accurate Biotechnology, China) and an Agilent RT-qPCR System (Agilent, USA). The measurement of the reactions was performed three times.

Western Blotting Analyses

The hDPSCs were cultured with OM, 1/32 MNPs eOM, and 1/32 Li-MNPs eOM in each of the 6-well plates for certain time points. The cells were lysed for protein extraction in RIPA lysis buffer (Beyotime, China) supplemented with PMSF

Table 2 Primers Used for RT-qPCR

Gene	Forward Primer (5'-3')	Reverse Primer (5'-3')
DSPP	GCTGGAAGCAATAACAGTACAG	TGCTGTTGATCTGAGGTGTTAT
DMP-1	CAAAGAAGATAGCAACTCCACG	CATCAACTGTTAATTTCCGGCT
ALP	ACTCTCCGAGATGGTGGTGGTG	CGTGGTCAATTCTGCCTCCTTCC
Runx2	AGGCAGTTCCCAAGCATTTCATCC	TGGCAGGTAGGTGTGGTAGTGAG
GAPDH	TGACATCAAGAAGGTGGTGAAGCAG	GTGTCGCTGTTGAAGTCAGAGGAG

(Beyotime, China) for 30 min on ice. The measurement of protein concentration was carried out using a BCA protein assay kit (Beyotime, China) based on the manufacturer's instructions. The total protein (20 μg) was separated using an SDS-PAGE gel and then transferred to a 0.45 μm PVDF membrane (Millipore, USA). Membrane blocking was conducted with 5% non-fat milk for 1 h, and the incubation was conducted with primary antibodies [anti-DSPP (1:1000, Proteintech, USA), anti-DMP-1 (1:1000, Bioss, China), anti-GSK3β (1:2000, Proteintech, USA), Anti-p-GSK3β (1:1000, Cell Signaling Technology, USA), anti-β-catenin (1:10,000, Proteintech, USA) and anti-GAPDH (1:20,000, Proteintech, USA)] overnight at 4 °C and with horse radish peroxidase (HRP)-linked secondary antibodies [Anti-Rabbit IgG (H+L) (1:2000, Proteintech, USA) and anti-Mouse IgG (H+L) (1:2000, Proteintech, USA)] for 1 h at room temperature. The protein bands were then visualized using a BeyoECL Star (Beyotime, China), and the quantification was conducted using ImageJ software (National Institutes of Health, USA). All protein expression levels were normalized to a GAPDH internal control.

In vitro Antibacterial Studies

In vitro antibacterial studies were performed using cariogenic bacteria, *S. mutans* (UA159, ATCC, USA). The culturing of *S. mutans* was performed in a brain–heart infusion (BHI) (Oxoid, Canada) medium. The growth of all bacterial samples was carried out under standardized anaerobic conditions for scheduled times at 37 °C.

The antibacterial effects of MNPs and Li-MNPs were determined using (i) colony formation assays and (ii) bacterial proliferation tests. Briefly, 100 mg MNPs or Li-MNPs were mixed with 100 μL PBS (1×), and a column of φ 6 mm × 3 mm was formed using a mold to simulate the morphology of the pulp capping agent. Then, these samples were dried at ambient temperature for 24 h. The UV-sterilized samples were placed in 24-well plates and exposed to *S. mutans* under standard anaerobic conditions for 24 h. For the control group, 10 μL PBS (10×) was added to each well to control for the effect of phosphate. In case (i), the samples were transferred into test tubes containing 5 mL of BHI medium, followed by ultrasonicating for 10 min. The suspension containing dissociated bacteria was serially diluted with BHI medium, and the seeding of a 100 μL aliquot of the diluted sample onto a BHI culture plate was performed for further incubation. In case (ii), bacterial proliferation was detected using the WST-8 reagent (Roche, Germany).[30] A total of 90 μL of BHI medium per well from a 24-well plate was transferred to a 96-well plate. After incubation with WST-8 reagent (diluted 1:10 with PBS) for 2 h at 37°C without light, the absorbance was recorded at 450 nm, and the OD was recorded to determine bacterial viability (n=3).

Animal Studies

For the in vivo study, a clinically relevant dental pulp exposure model was employed as described elsewhere.[31,32] These experiments were performed following the approval from the Institutional Animal Care and Use Committee of Guangdong Huawei Testing Co., LTD (approval number: 202208004) and complied with the Guide for Care and Use of Laboratory Animals. Twelve 6-week-old male C57BL/6 mice (18–22 g) were used (Bestest, China). The mice were divided into four groups: Blank, MNPs, Li-MNPs, and MTA (maxillary first molars, n=6). The animals were anesthetized with general anesthetic according to the manufacturer's instructions [Zoletil 50 (Virbac, France), Sumianxin II (ShengXin, China)]. Vital pulp therapy of the maxillary first molars in mice was performed using a microscope (Leica, Germany), a medical ultrasonic apparatus (Piezon Master 700, EMS, Swiss), and a dental bur (TC-21EF, MANI, Japan). The material was mixed well with DW (1:1 wt), then 2 mg of the mixture was added to the pulp exposure in each tooth. Then, the cavity was sealed with resin (Dyad FlowTM, Kerr, USA) to prevent microbial leakage. The blank group used only sterile cotton balls placed on the dental defect.

The mice were sacrificed after 4 weeks. Samples were fixed using 4% PFA for 48 h. After the dissection of the maxillae, the teeth were collected for scanning using a micro-CT scanner (Skyscan 1172, Bruker, Germany). After scanning, NRecon and DataViewer software (Bruker, Germany) were employed for standard reconstruction. The reparative dentin volume/total volume (RDV/TV) was measured and calculated using CTvox and CTAn software (Bruker, Germany) (n=5). For histological analysis, the teeth were decalcified with EDTA (Sangon Biotech, China) for 4 weeks after micro-CT scanning. After decalcification, the teeth were paraffin-embedded. Hematoxylin and eosin (H&E) staining was performed using 4 μm thick tissue sections. These procedures were performed in accordance with the

manufacturer's instructions. The area of reparative dentin and the number of blood vessels in the pulp chamber were counted using ImageJ software (n=5).

Statistical Analysis

All data were recorded as means ± standard deviations. One-way ANOVAs were performed to analyze the differences between groups, and the Student's *t*-test was employed to assess the significance of these differences. Differences with $p<0.05$ were regarded as statistically significant.

Results and Discussion

Li-MNPs were synthesized using an alkali-catalyzed sol-gel method described previously.[27] As can be seen in the results of TOF-SIMS, the surfaces of Li-MNPs uniformly feature punctated light spots, indicating that lithium has been incorporated uniformly into the MNPs (Figure 1A and B). SEM and TEM analyses of Li-MNPs revealed that they are spherical with a particle size of approximately 520 nm and a rough and porous surface (Figure 2A and C). The determined zeta potential values were −14.7 ± 0.10 mV for Li-MNPs and −19.63 ± 0.36 mV for MNPs (Figure 2D). These results provide compelling evidence of the successful removal of CTAB, encompassing a positively charged hydrophilic group. According to the SEM findings, the hydrated particle size of Li-MNPs is marginally smaller than that of MNPs (Figure 2E). To further characterize the pore structure of Li-MNPs, they were tested using the BET and BJH approaches, and the results are outlined in Table 3. Li-MNPs exhibit a greater specific surface area (172.38 m^2/g), smaller pore volume (0.23 cm^3/g), and reduced pore size (4.81 nm) than MNPs. The N_2 adsorption–desorption curve is classified as a Type IV isotherm under the IUPAC system and closely resembles an H2b-type hysteresis loop (Figure 3A and B). This result and the pore size indicate the presence of mesoporous structures in Li-MNPs.[33] XRD is capable of demonstrating alterations in the crystal structure pre- and post-lithium doping. Li-MNPs exhibit broad peaks that match the characteristics of silicate glass,[34] implying that Li-MNPs retain an amorphous structure when doped with 5% lithium (Figure 3C). The FT-IR spectra of Li-MNPs manifest absorption peaks typical of Si–O–Si bonds at approximately 1088 cm^{-1}, 802 cm^{-1}, and 476 cm^{-1} (Figure 3D).[35] Furthermore, the peaks observed at 3452 cm^{-1} and 1637 cm^{-1} are attributable to O–H stretching vibrations, indicative of the material's absorption of atmospheric moisture. These observations align seamlessly with the quintessential attributes of bioactive glass-based MNPs.

The ionic release behavior of Li-MNPs was then subsequently investigated. Figure 4 displays the variations in Ca, Si, P and Li ion concentrations in Tris-HCl solution at different soaking times. The total Ca ion release is higher in MNPs than in Li-MNPs, which reflects the different Ca ion concentrations in these two glass structures. Due to mineralization, Ca and P ion concentrations decreased in the MNP and Li-MNP groups with a similar trend.[36] Interestingly, the concentration of Li ions also showed a decreasing trend at a later stage, suggesting that Li ions may also be involved in forming calcium phosphate. Based on the amount of Ca, Si, P, and Li ions released, Li-MNPs are expected to influence the cellular regenerative response, as these ions have been shown to significantly stimulate stem cell and endothelial cell functions.[37]

Therefore, the biological effects of Li-MNPs were investigated using hDPSCs, resident cells on the dental pulp susceptible to bacterial infection, which play an important role in tissue regeneration.[38,39] We first identified these cells using flow cytometry and immunofluorescence. The results showed that these cells expressed high levels of mesenchymal stem cell surface markers and low levels of vascular and endothelial cell surface markers, indicating high-purity hDPSCs (Figure 5A and B). The biocompatibility of Li-MNPs was then assessed using the CCK-8 assay. Cells were treated for 7 days with different concentrations of material extracts and at relatively high concentrations (1/128-1/8, 1.5625–25 mg/mL). Extracts of both MNPs and Li-MNPs did not affect cell activity (Figure 6A). The inhibitory effect of Li-MNPs on cell proliferation was more evident at the 1/4 concentration (50 mg/mL). This was possibly due to the toxicity of the cells caused by a higher concentration of Li ions. Zhao et al showed that MTA extracts were significantly toxic to hDPSCs at 10 mg/mL concentrations.[40] In contrast, Li-MNPs were not cytotoxic at this concentration, suggesting that Li-MNPs exhibit low cytotoxicity and good biocompatibility. Notably, similar to a study by Han et al,[24] Li-MNPs did not promote cell proliferation, which may be a result of the effect of lithium on the cell cycle.[41] Overall, based on the cell proliferation and vitality studies, we concluded that Li-MNPs displayed acceptable cytocompatibility

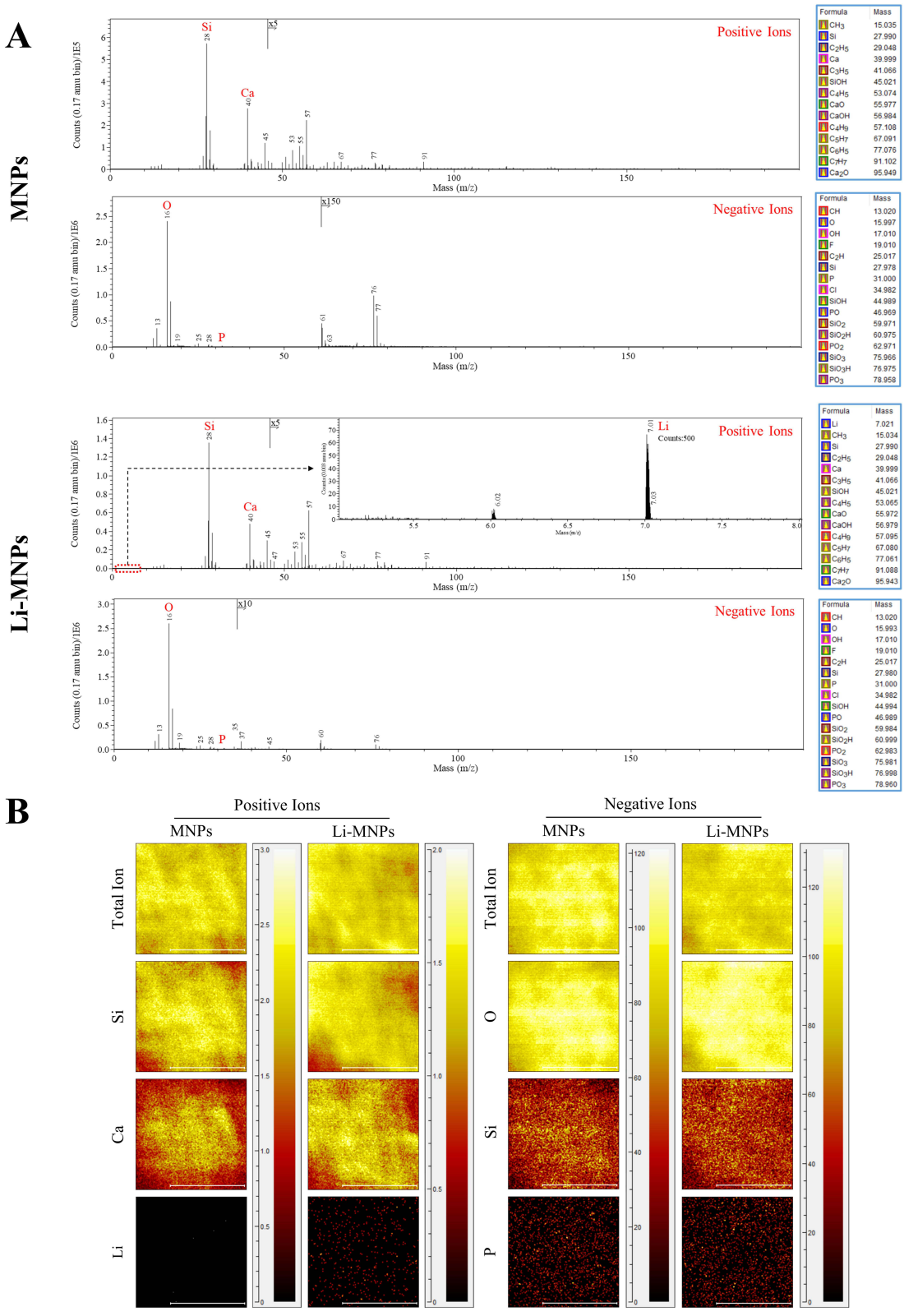

Figure 1 The elemental composition of MNPs and Li-MNPs. (**A**) The mass spectra. (**B**) The ion mapping.

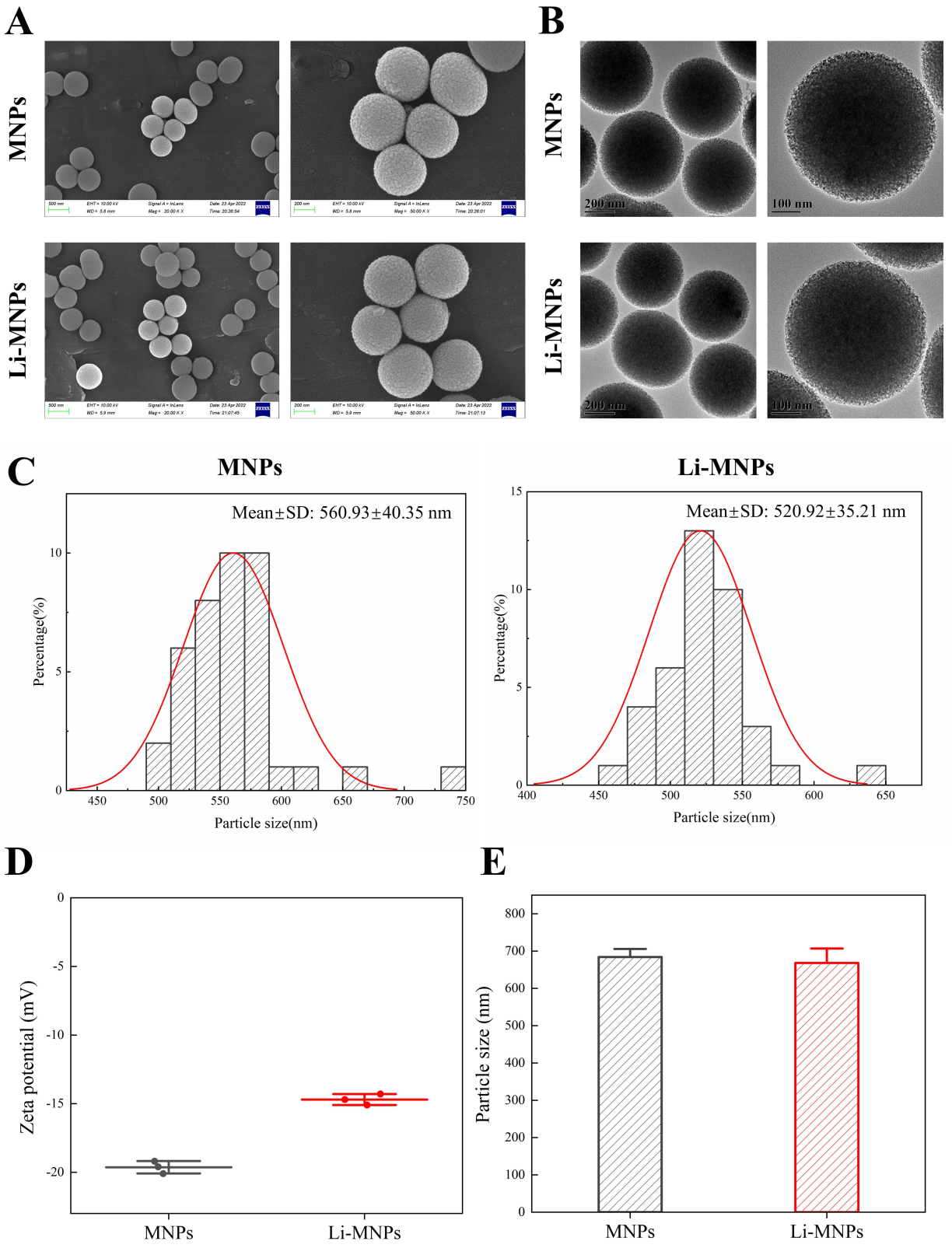

Figure 2 The surface morphology, zeta potential, and particle size of MNPs and Li-MNPs. (**A**) The SEM images. Scale bar = 500; 200 μm. (**B**) The TEM images. Scale bar = 200; 100 μm. (**C**) Particle size analyzed by SEM images. (**D**) Zeta potential. (**E**) Hydrodynamic size.

Table 3 The Textural Characteristics of MNPs and Li-MNPs

Sample	Surface Area (m^2g^{-1})	Average Pore Diameter (nm)	Pore Volume (cm^3g^{-1})
MNPs	172.38	5.25	0.23
Li-MNPs	221.78	4.81	0.25

and might be suitable as a pulp capping agent. Guided by the outcomes of the CCK-8 assay, subsequent experiments were undertaken with extract concentrations ranging between 1/128 to 1/8.

We subsequently examined the impact of Li-MNPs on the differentiation of hDPSCs, assessing ALP activity, mineralization, and both gene and protein expression levels. ALP is an early osteogenic or odontogenic differentiation marker that participates in pre-mineralization and promotes the formation of mineral nodules.[42] After 7 days, an elevated expression level of ALP was evident within the Li-MNP extract at a concentration of 1/32 (Figure 6B and C). This contrasts with the MNP extract at an equivalent concentration and the control groups, as ascertained through ALP staining and subsequent quantitative analysis. Concurrently, calcium deposition, a vital indicator of odontogenic differentiation, peaks in the late phases of odontogenesis.[43] An ARS assay conducted after 21 days confirmed that Li-MNPs fostered the formation of mineralized nodules that were denser and larger than those resulting from MNPs treatment, underlining Li-MNPs exemplary odontogenic induction capabilities (Figure 6D).

The effect of the 1/32 concentration of MNP and Li-MNP extracts on the expression of odontogenic-related genes in hDPSCs was further examined using RT-qPCR. The expression levels of genes related to odontogenesis, namely DSPP, DMP-1, ALP, and Runx2, were found to be significantly higher after 7 days of treatment with Li-MNPs compared with both the control and MNPs ($p<0.05$) (Figure 7A). Considering that lithium doping greatly improves the odontogenic

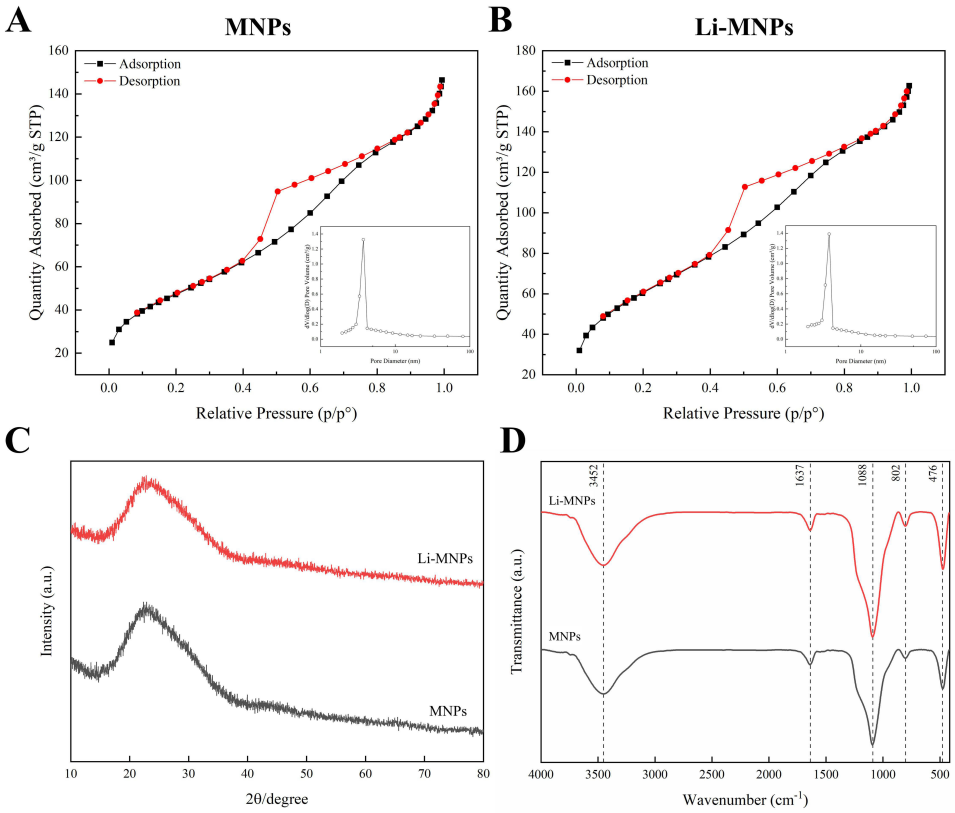

Figure 3 Pore structure and chemical structure analysis of MNPs and Li-MNPs. (**A**) N_2 adsorption–desorption isotherms and the pore size distribution of MNPs. (**B**) N_2 adsorption–desorption isotherms and the pore size distribution of Li-MNPs. (**C**) XRD pattern. (**D**) FT-IR spectra.

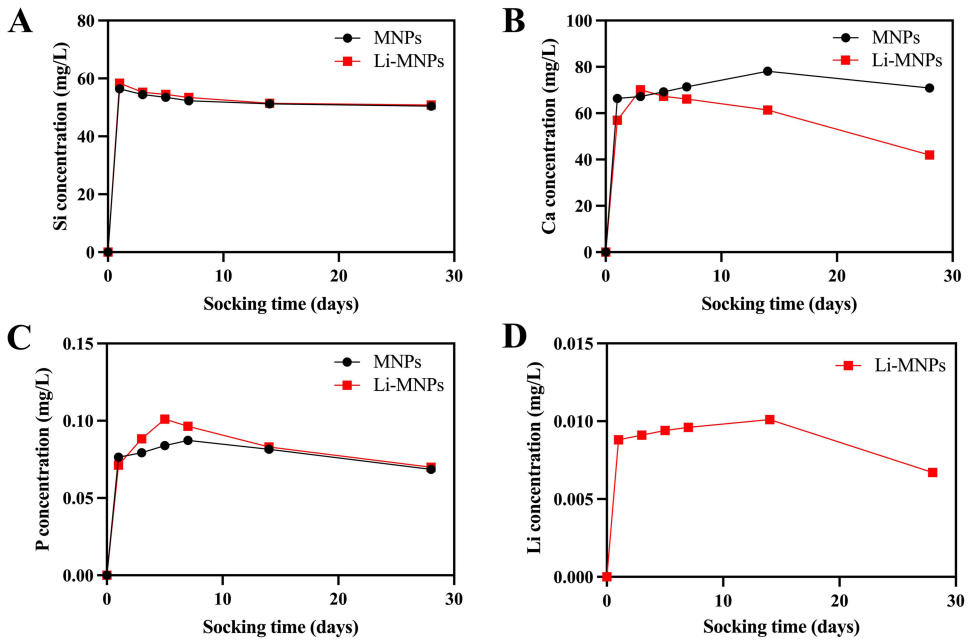

Figure 4 Ion release from MNPs and Li-MNPs in Tris-HCl solution. (**A**) Si ions. (**B**) Ca ions. (**C**) P ions. (**D**) Li ions.

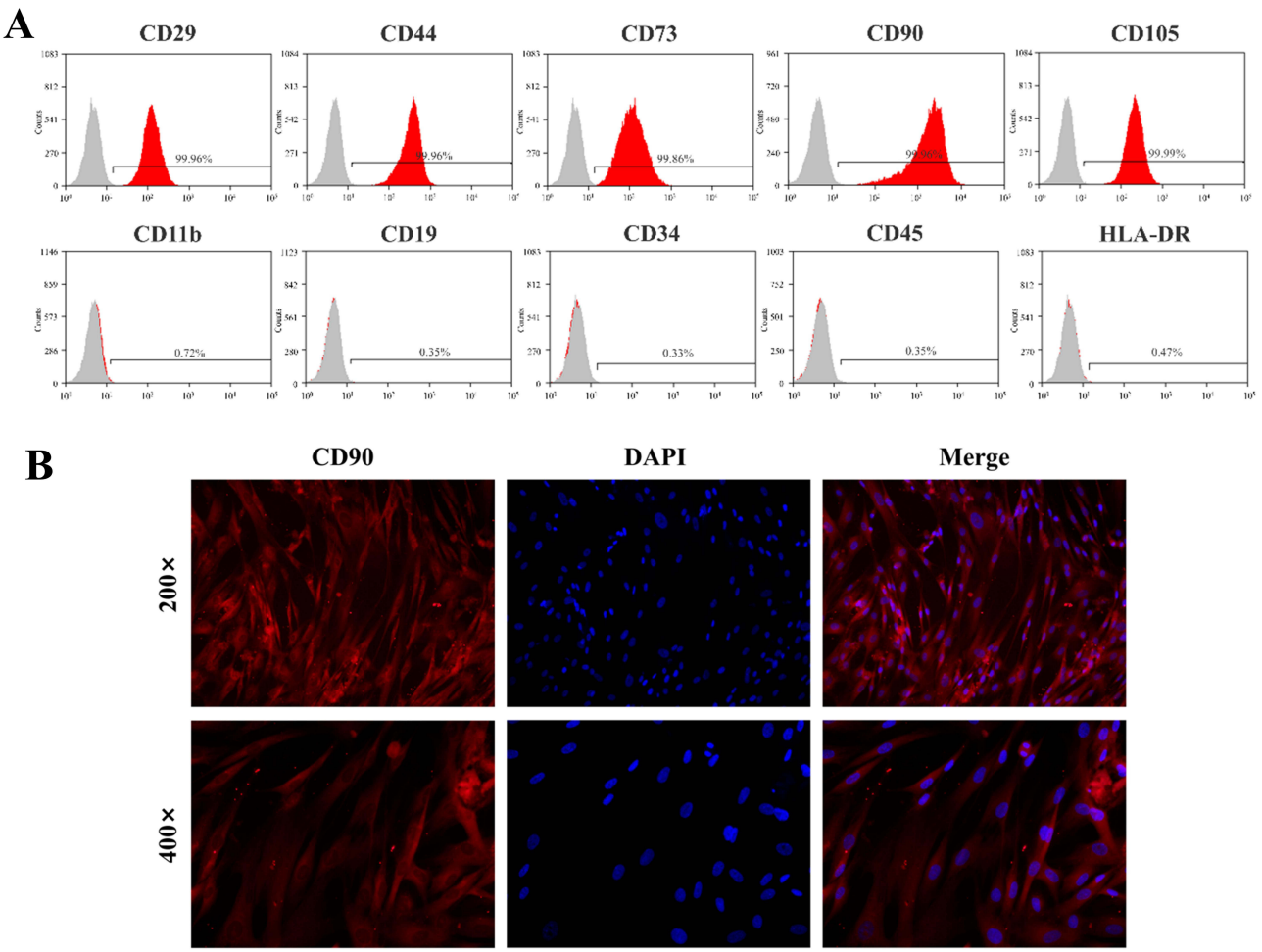

Figure 5 Identification of hDPSCs. (**A**) Flow cytometry of cells. (**B**) Immunofluorescence of cells.

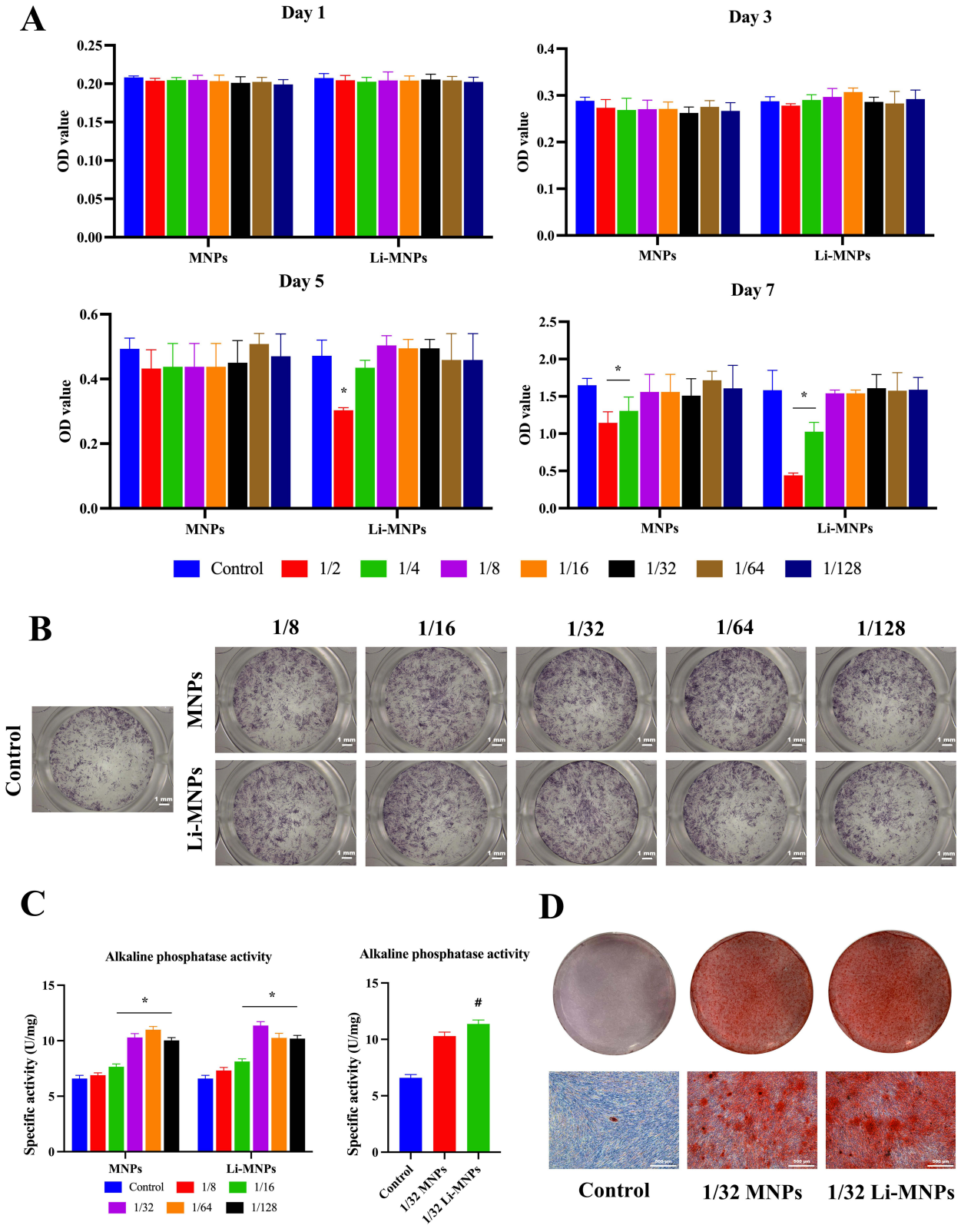

Figure 6 Cytotoxicity and odontogenic induction effects of MNPs and Li-MNPs. (**A**) CCK-8 assay for the proliferation of hDPSCs cultured in varying concentrations of MNP and Li-MNP extracts for 1, 3, 5, and 7 days. (**B**) ALP staining of MNP and Li-MNP extracts stimulated hDPSCs after 7 days. Scale bar = 1 mm. (**C**) ALP activity quantification of MNP and Li-MNP extracts stimulated hDPSCs after 7 days. (**D**) ARS after 21 days of stimulation. Scale bar = 500 μm. *Indicates significant differences compared with the control group; #Indicates significant differences compared with the MNP group, $p < 0.05$.

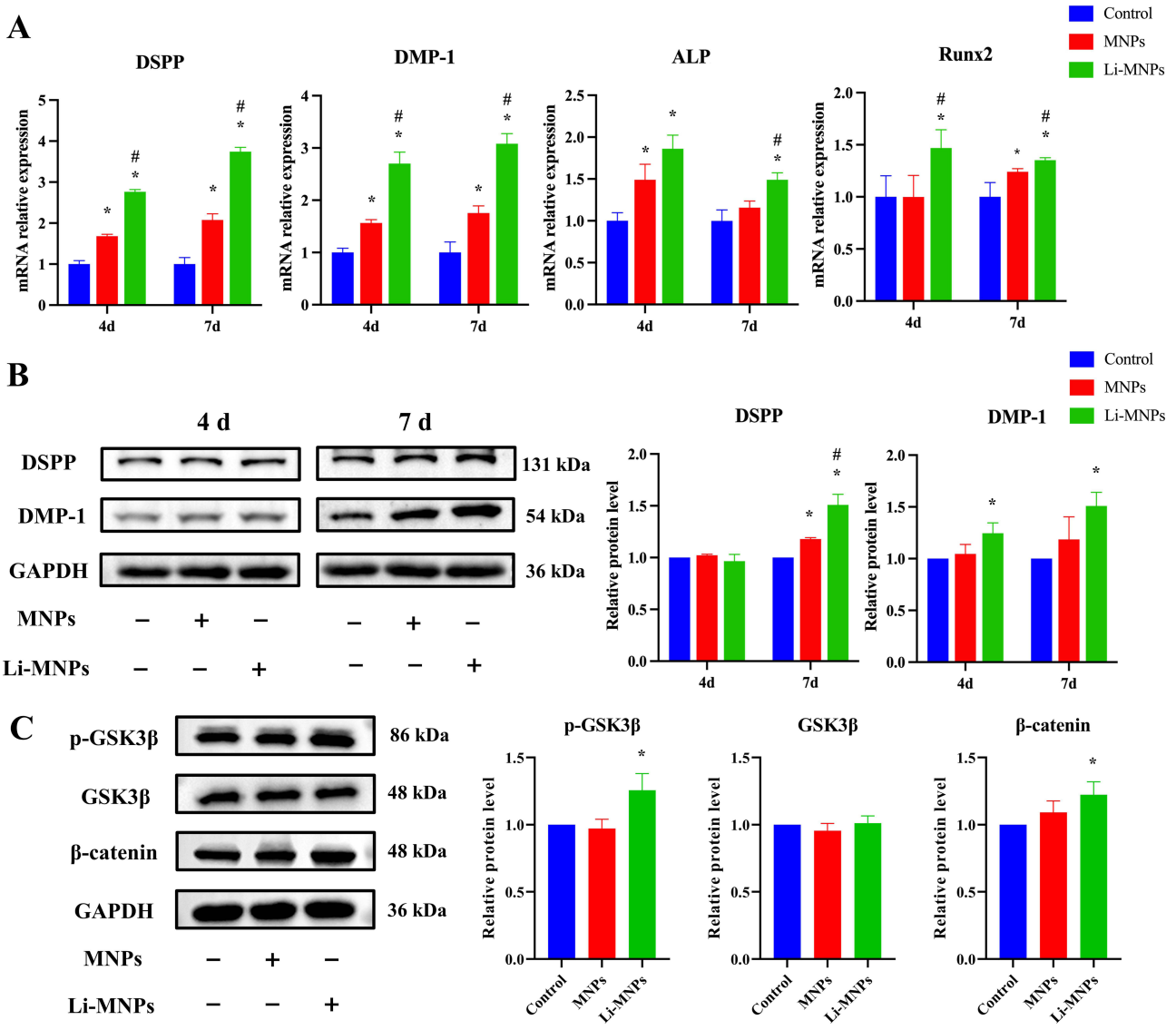

Figure 7 The regulatory effects of MNPs and Li-MNPs on genes and proteins. (**A**) RT-qPCR analysis of odontogenesis-related genes (DSPP, DMP-1, ALP, Runx2) for hDPSCs cultured in MNP and Li-MNP extracts for 4 and 7 days. (**B**) Western blotting assay for DSPP and DMP-1 in hDPSCs cultured in MNP and Li-MNP extracts for 4 and 7 days. (**C**) Western blotting assay for GSK3β, p-GSK3β, and β-catenin in hDPSCs cultured in MNP and Li-MNP extracts for 7 days. *Indicates significant differences compared with the control group; #Indicates significant differences compared with the MNP group. $p < 0.05$.

properties of MNPs. The expression of dentin-associated proteins was further explored to confirm the ALP, ARS, and gene analyses. As expected, the Li-MNP extract significantly enhanced the expression of DMP-1 on Day 4 and DSPP and DMP-1 on Day 7, compared with the control group ($p<0.05$) (Figure 7B).

This led us to probe the mechanism behind lithium's potentiation of odontogenic expression within hDPSCs. Given the pivotal role of Wnt signaling in tooth development and lithium's status as a GSK-3β inhibitor,[25,44] we delved into the Wnt/β-catenin signaling pathway's activation post a 7-day Li-MNPs stimulation of hDPSCs using a Western blotting assay. Li-MNPs significantly enhanced the expression of p-GSK3β and β-catenin compared with the control and MNPs ($p<0.05$), suggesting that Li-MNPs have the ability to activate the Wnt/β-catenin signaling pathway by promoting the phosphorylation of GSK-3β, leading to the accumulation of β-catenin (Figure 7C). The results above demonstrate that Li-MNPs play a role in promoting the odontogenic differentiation of hDPSCs by activating the Wnt/β-catenin signaling pathway.

The regeneration of infected pulp tissues is a challenging topic in dentistry.[45] *S. mutans*, an endogenous oral microflora component, has long been involved in the etiology of dental caries.[46,47] In addition to assessing the pulp capping agent

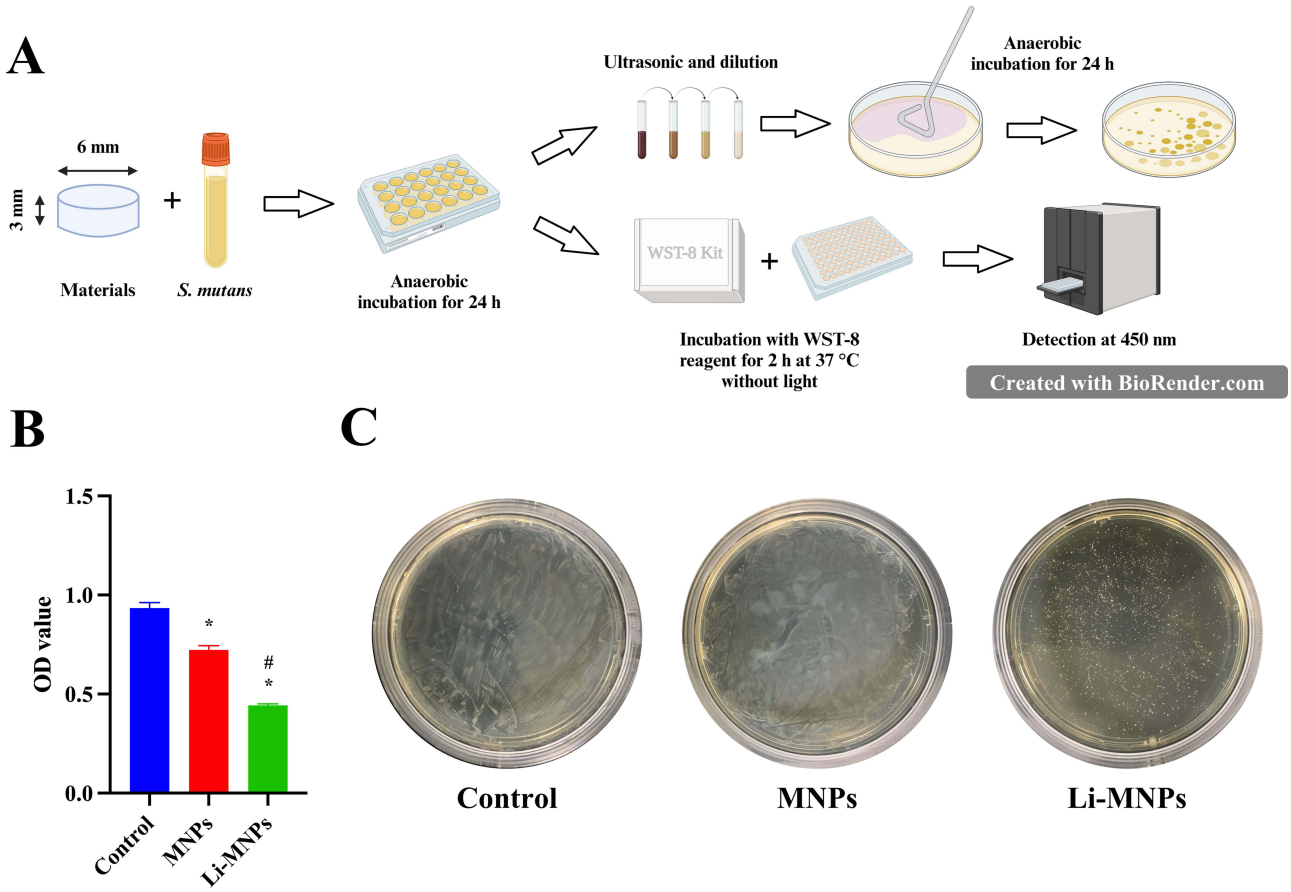

Figure 8 In vitro antibacterial studies. (**A**) Schematic illustration of the antibacterial experiment (Created with Biorender.com). (**B**) Bacterial proliferation test. (**C**) Colony formation assay. *Indicates significant differences compared with the control group; #Indicates significant differences compared with the MNP group. $p < 0.05$.

functions of Li-MNPs, the antibacterial property was investigated (Figure 8A). As shown in Figure 8B and C, both MNPs and Li-MNPs inhibited the growth of *S. mutans*, with Li-MNPs showing a more pronounced inhibitory effect ($p<0.05$). We speculate that the antibacterial effect may be due to the synergistic effects of bioactive glass-based MNPs and Li ions. Bioactive glasses have been reported to inhibit *S. mutans* by releasing Ca and Si ions, which react with hydrogen ions in a protonation reaction, raising the pH of the solution and increasing the osmotic pressure of the solution.[48–51] Keikhosravani et al have reported various antibacterial effects of Li ions.[52] Li ions with a positive charge bind to bacterial cell walls with a negative charge, and this disrupts the cell wall, leading to the release of cytoplasmic contents and dehydration.[53,54] This can also further contribute to the antibacterial effects of biologically active glasses. Additionally, Li ions disrupt the polynucleotide chains of both DNA and RNA, influencing enzyme function by changing protein conformations.[53,55]

Based on these observations, our next objective was to confirm the in vivo effect of Li-MNPs in promoting dentin regeneration in situ. For this, mouse dental pulp exposure was modeled (Figure 9A).[31,32] MNPs, Li-MNPs, and MTA were used for pulp capping. The blank group was used as a negative control, and the MTA group was used as a positive control. The impact of dentin regeneration in every group was evaluated as previously reported.[56] Samples were collected and scanned using micro-CT four weeks after the operation. Representative section view images of each group were obtained (Figure 9B). The blue and green areas correspond to resin and enamel, respectively. The orange and purple areas correspond to dentin. As anticipated, there was almost no formation of reparative dentin in the control group and only partial formation of reparative dentin in the MNP group. The continuous formation of reparative dentin on the tooth's pulp defect was observed in the Li-MNP group, akin to the results obtained in the MTA group. To measure the efficiency of dentin regeneration, these data were reconstructed in three dimensions, analysed, and the RDV/TV for each group determined, as shown in Figure 9D. Li-MNPs and MTA exhibited higher RDV/TV values, indicating that Li-MNPs

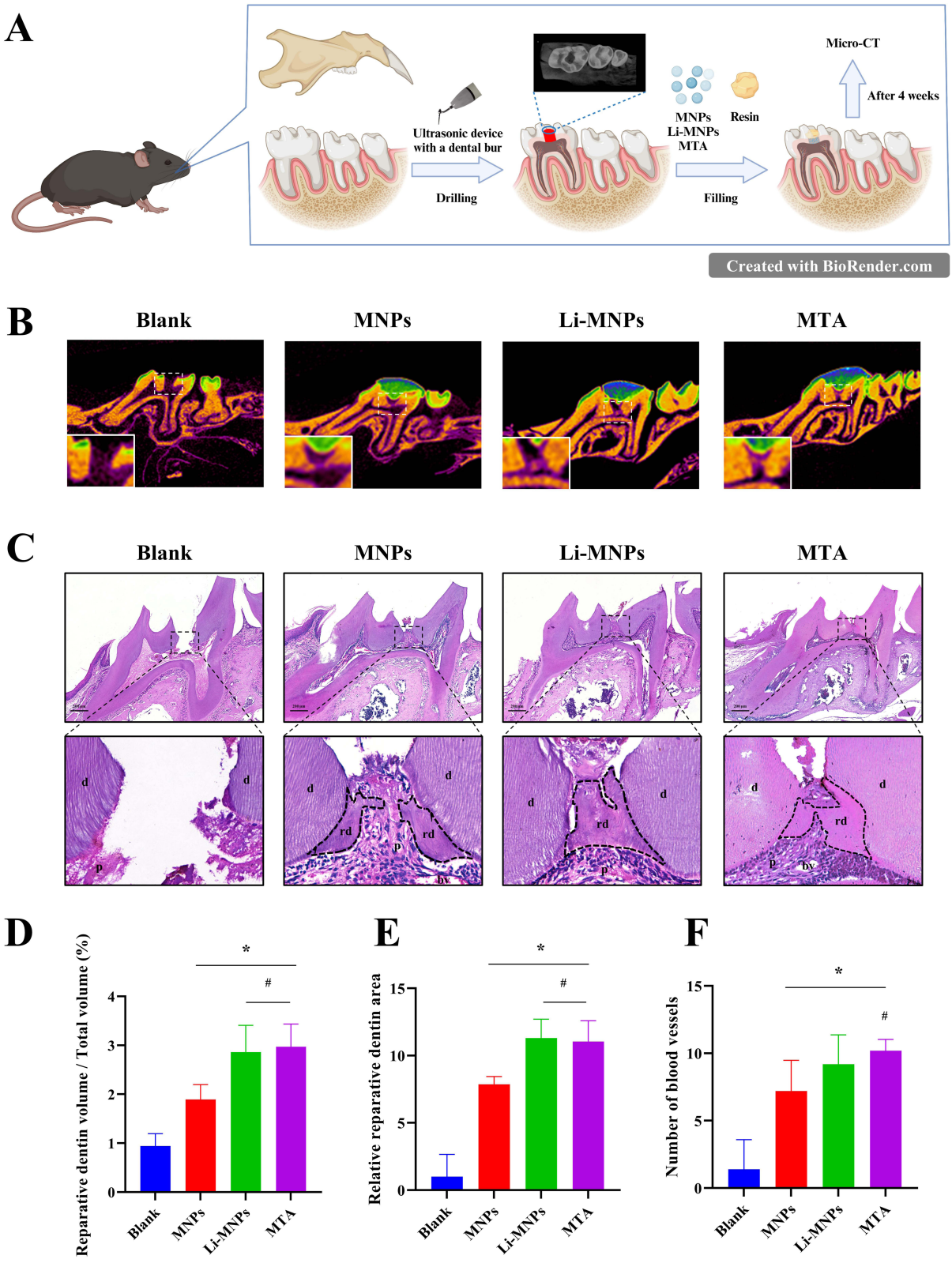

Figure 9 In vivo evaluation. (**A**) Scheme of the animal modeling: a mouse molar tooth defect, filled with Li-MNPs and resin, and 4 weeks post-operation, micro-CT analysis was performed to observe the regeneration of reparative dentin; for comparison, MTA served as a commercial pulp regenerative dental material, and MNPs were also used (Created with Biorender.com). (**B**) Micro-CT representative section view images. (**C**) H&E staining. Scale bar = 200 μm. p: dental pulp. rd: reparative dentin. d: native dentin. bv: blood vessel. (**D**) Reparative dentin volume/total volume (%). n=5. (**E**) Relative reparative dentin area. n=5. (**F**) Number of blood vessels. n=5. *Indicates significant differences compared with the blank group; #Indicates significant differences compared with the MNP group. $p < 0.05$.

possess a comparable ability to stimulate dentin regeneration to that of MTA. The tissue samples were examined histologically following H&E staining to analyze the characteristics of the hard tissues formed within the pulp chamber. As shown in Figure 9C, the blank group exhibited liquefaction and necrosis of the pulp due to pulp cavity exposure where no reparative dentin on the top of the pulp chamber was formed. In the MNP group, there was some formation of reparative dentin, but it was discontinuous. On the other hand, both the Li-MNP and MTA groups formed continuous reparative dentin, resulting in better regenerative capacity. Subsequently, the reparative dentin area and the number of blood vessels in the pulp chamber were evaluated in each group (Figure 9E and F). In the Li-MNP and MTA groups, a greater amount of reparative dentin and blood vessels formed compared with the blank and MNP groups ($p<0.05$). In summary, Li-MNPs combine the advantages of bioactive glass and lithium, integrating the biological effects of lithium to further enhance its bioactivity and antibacterial capacity, while maintaining the original biocompatibility as much as possible. Through in vivo experiments, a single concentration and dose of Li-MNPs were used for pulp capping, and the results showed that Li-MNPs have an excellent ability to contribute to dentin regeneration, suggesting that Li-MNPs are highly suitable for dental applications and have great clinical potential. However, the optimal concentration of Li-MNPs for in vivo application is unknown, and it is necessary to further investigate the effects of different doses of Li-MNPs on dentin regeneration in vivo to provide a further theoretical basis for achieving clinical translation.

Conclusion

In this study, the successful synthesis and comprehensive characterization of Li-MNPs were achieved. The release of lithium, calcium, silicon, and phosphorus ions from Li-MNPs remarkably enhanced the odontogenic differentiation and mineralization of hDPSCs. The activation of the Wnt/β-catenin signaling pathway via the induction of GSK-3β phosphorylation, prompted by the presence of lithium, underscores the pivotal role of lithium in enhancing odontogenic expression within hDPSCs. We also demonstrated that Li-MNPs significantly curtail the growth of *S. mutans*, a primary perpetrator of dental caries. Finally, our in vivo experiments mirrored the in vitro results, showcasing the ability of Li-MNPs to foster dentin regeneration comparably to MTA. Given these multifaceted advantages, Li-MNPs exhibit immense clinical potential in dentistry and stand out as a promising candidate for broader applications in regenerative medicine.

Acknowledgments

This work was supported by the Science and Technology Planning Project of Guangdong Province (2021A0505030079), Special Foundation of Science and Technology Innovation Strategy of Guangdong Province (2021A1515010870) and the Science and Technology Planning Project of Guangzhou Liwan District of Guangdong Province (2201006). Figures 8A and 9A were created with BioRender.com. We thank Charlesworth Author Services for its linguistic assistance during the preparation of this manuscript.

Disclosure

The authors report no conflicts of interest in this work.

References

1. Zhang W, Yelick PC. Tooth repair and regeneration: potential of dental stem cells. *Trends Mol Med*. 2021;27(5):501–511. doi:10.1016/j.molmed.2021.02.005
2. Marrelli M, Codispoti B, Shelton RM, et al. Dental pulp stem cell mechanoresponsiveness: effects of mechanical stimuli on dental pulp stem cell behavior. *Front Physiol*. 2018;9:1685. doi:10.3389/fphys.2018.01685
3. Duncan HF, Kobayashi Y, Kearney M, Shimizu E. Epigenetic therapeutics in dental pulp treatment: hopes, challenges and concerns for the development of next-generation biomaterials. *Bioact Mater*. 2023;27:574–593. doi:10.1016/j.bioactmat.2023.04.013
4. Fulzele P, Baliga S, Thosar N, Pradhan D. Evaluation of calcium ion, hydroxyl ion release and pH levels in various calcium hydroxide based intracanal medicaments: an in vitro study. *Contemp Clin Dent*. 2011;2(4):291–295. doi:10.4103/0976-237X.91791
5. Njeh A, Uzunoğlu E, Ardila-Osorio H, et al. Reactionary and reparative dentin formation after pulp capping: hydrogel vs. Dycal. *Evid Based Endod*. 2016;1(1):3. doi:10.1186/s41121-016-0003-9
6. Mente J, Michel A, Panagidis D. Treatment outcome of mineral trioxide aggregate or calcium hydroxide direct pulp capping: long-term results. *Clin Res*. 2014;2014:6.
7. Markovic D, Zivojinovic V, Vucetic M. Evaluation of three pulpotomy medicaments in primary teeth. *Eur J Paediatr Dent*. 2005;6:3.

8. Roberts HW, Toth JM, Berzins DW, Charlton DG. Mineral trioxide aggregate material use in endodontic treatment: a review of the literature. *Dent Mater*. 2008;24(2):149–164. doi:10.1016/j.dental.2007.04.007
9. Lucas C, Viapiana R, Bosso-Martelo R, Guerreiro-Tanomaru JM, Camilleri J, Tanomaru-Filho M. Physicochemical properties and dentin bond strength of a tricalcium silicate-based retrograde material. *Braz Dent J*. 2017;28(1):51–56. doi:10.1590/0103-6440201701135
10. Stringhini Junior E, Dos Santos MGC, Oliveira LB, Mercadé M. MTA and biodentine for primary teeth pulpotomy: a systematic review and meta-analysis of clinical trials. *Clin Oral Invest*. 2019;23(4):1967–1976. doi:10.1007/s00784-018-2616-6
11. Jafari F, Samadi Kafil H, Jafari S, Aghazadeh M, Momeni T. Antibacterial Activity of MTA Fillapex and AH 26 root canal sealers at different time intervals. *Iran Endod J*. 2016;11(3):192–197. doi:10.7508/iej.2016.03.009
12. Mohammadi Z, Shalavi S. Effect of hydroxyapatite and bovine serum albumin on the antibacterial activity of MTA. *Iran Endod J*. 2011;6 (4):136–139.
13. Kim RJY, Kim MO, Lee KS, Lee DY, Shin JH. An in vitro evaluation of the antibacterial properties of three mineral trioxide aggregate (MTA) against five oral bacteria. *Arch Oral Biol*. 2015;60(10):1497–1502. doi:10.1016/j.archoralbio.2015.07.014
14. Al-Hezaimi K, Al-Shalan TA, Naghshbandi J, Oglesby S, Simon JHS, Rotstein I. Antibacterial effect of two mineral trioxide aggregate (MTA) preparations against enterococcus faecalis and streptococcus sanguis in vitro. *J Endod*. 2006;32(11):1053–1056. doi:10.1016/j.joen.2006.06.004
15. Jain AS, Gupta AS, Agarwal R. Comparative evaluation of the antibacterial activity of two Biocompatible materials i.e. Biodentine and MTA when used as a direct pulp capping agent against streptococcus mutans and Enterococcus faecalis- An in vitro study. *Endodontology*. 2018;30(1):66. doi:10.4103/endo.endo_66_17
16. Kazemian Z, Varzandeh M, Labbaf S. A facile synthesis of mono dispersed spherical silver doped bioactive glass nanoparticle. *J Mater Sci Mater Med*. 2021;32(3):29. doi:10.1007/s10856-021-06496-9
17. Polo-Montalvo A, Casarrubios L, Serrano MC, et al. Effective actions of ion release from mesoporous bioactive glass and macrophage mediators on the differentiation of osteoprogenitor and endothelial progenitor cells. *Pharmaceutics*. 2021;13(8):1152. doi:10.3390/pharmaceutics13081152
18. Garrido-Cano I, Adam-Artigues A, Lameirinhas A, et al. Delivery of miR-200c-3p using tumor-targeted mesoporous silica nanoparticles for breast cancer therapy. *ACS Appl Mater Interfaces*. 2023;15(32):38323–38334. doi:10.1021/acsami.3c07541
19. Zhang Y, Wei L, Chang J, et al. Strontium-incorporated mesoporous bioactive glass scaffolds stimulating in vitro proliferation and differentiation of bone marrow stromal cells and in vivo regeneration of osteoporotic bone defects. *J Mater Chem B*. 2013;1(41):5711–5722. doi:10.1039/C3TB21047B
20. Mousa M, Milan JA, Kelly O, et al. The role of lithium in the osteogenic bioactivity of clay nanoparticles. *Biomater Sci*. 2021;9(8):3150–3161. doi:10.1039/D0BM01444C
21. Kargozar S, Montazerian M, Hamzehlou S, Kim HW, Baino F. Mesoporous bioactive glasses: promising platforms for antibacterial strategies. *Acta Biomaterialia*. 2018;81:1–19. doi:10.1016/j.actbio.2018.09.052
22. Zhang K, Alaohali A, Sawangboon N, Sharpe PT, Brauer DS, Gentleman E. A comparison of lithium-substituted phosphate and borate bioactive glasses for mineralised tissue repair. *Dent Mater*. 2019;35(6):919–927. doi:10.1016/j.dental.2019.03.008
23. Clément-Lacroix P, Ai M, Morvan F, et al. Lrp5-independent activation of Wnt signaling by lithium chloride increases bone formation and bone mass in mice. *Proc Natl Acad Sci USA*. 2005;102(48). doi:10.1073/pnas.0505259102
24. Han P, Wu C, Chang J, Xiao Y. The cementogenic differentiation of periodontal ligament cells via the activation of Wnt/β-catenin signalling pathway by Li+ ions released from bioactive scaffolds. *Biomaterials*. 2012;33(27):6370–6379. doi:10.1016/j.biomaterials.2012.05.061
25. Ali M, Okamoto M, Komichi S, et al. Lithium-containing surface pre-reacted glass fillers enhance hDPSC functions and induce reparative dentin formation in a rat pulp capping model through activation of Wnt/β-catenin signaling. *Acta Biomaterialia*. 2019;96:594–604. doi:10.1016/j.actbio.2019.06.016
26. Lieb J. The immunostimulating and antimicrobial properties of lithium and antidepressants. *J Infect*. 2004;49(2):88–93. doi:10.1016/j.jinf.2004.03.006
27. Mao Y, Liao J, Wu M, et al. Preparation of nano spherical bioglass by alkali-catalyzed mixed template. *Mater Res Express*. 2020;7(10):105202. doi:10.1088/2053-1591/abc373
28. Chandra A, Lin T, Young T, et al. Suppression of sclerostin alleviates radiation-induced bone loss by protecting bone-forming cells and their progenitors through distinct mechanisms. *J Bone Miner Res*. 2017;32(2):360–372. doi:10.1002/jbmr.2996
29. Han P, Xu M, Chang J, Chakravorty N, Wu C, Xiao Y. Lithium release from β-tricalcium phosphate inducing cementogenic and osteogenic differentiation of both hPDLCs and hBMSCs. *Biomater Sci*. 2014;2(9):1230. doi:10.1039/C4BM00111G
30. Keum H, Kim D, Whang CH, et al. Impeding the medical protective clothing contamination by a spray coating of trifunctional polymers. *ACS Omega*. 2022;7(12):10526–10538. doi:10.1021/acsomega.1c04919
31. Song M, Kim S, Kim T, et al. Development of a direct pulp-capping model for the evaluation of pulpal wound healing and reparative dentin formation in mice. *J Vis Exp*. 2017;2017(119). doi:10.3791/55277
32. Du W, Yang M, Kim T, et al. Indigenous microbiota protects development of medication-related osteonecrosis induced by periapical disease in mice. *Int J Oral Sci*. 2022;14(1):16. doi:10.1038/s41368-022-00166-4
33. Thommes M, Kaneko K, Neimark AV, et al. Physisorption of gases, with special reference to the evaluation of surface area and pore size distribution (IUPAC Technical Report). *Pure Appl Chem*. 2015;87(9–10):1051–1069. doi:10.1515/pac-2014-1117
34. Lee JH, Kang MS, Mahapatra C, Kim HW. Effect of aminated mesoporous bioactive glass nanoparticles on the differentiation of dental pulp stem cells. *PLoS One*. 2016;11(3):e0150727. doi:10.1371/journal.pone.0150727
35. Arcos D, Vila M, López-Noriega A, et al. Mesoporous bioactive glasses: mechanical reinforcement by means of a biomimetic process. *Acta Biomaterialia*. 2011;7(7):2952–2959. doi:10.1016/j.actbio.2011.02.012
36. Mo Y, Zhao F, Lin Z, Cao X, Chen D, Chen X. Local delivery of naringin in beta-cyclodextrin modified mesoporous bioactive glass promotes bone regeneration: from anti-inflammatory to synergistic osteogenesis and osteoclastogenesis. *Biomater Sci*. 2022;10(7):1697–1712. doi:10.1039/D1BM01842F
37. Arcos D, Portolés MT. Mesoporous bioactive nanoparticles for bone tissue applications. *Int J Mol Sci*. 2023;24(4):3249. doi:10.3390/ijms24043249
38. Gronthos S, Mankani M, Brahim J, Robey PG, Shi S. Postnatal human dental pulp stem cells (DPSCs) in vitro and in vivo. *Proc Natl Acad Sci USA*. 2000;97(25):13625–13630. doi:10.1073/pnas.240309797

39. Zhang YD, Chen Z, Song YQ, Liu C, Chen YP. Making a tooth: growth factors, transcription factors, and stem cells. *Cell Res*. 2005;15(5):301–316. doi:10.1038/sj.cr.7290299
40. Zhao X, He W, Song Z, Tong Z, Li S, Ni L. Mineral trioxide aggregate promotes odontoblastic differentiation via mitogen-activated protein kinase pathway in human dental pulp stem cells. *Mol Biol Rep*. 2012;39(1):215–220. doi:10.1007/s11033-011-0728-z
41. Mehta PM, Gimenez G, Walker RJ, Slatter TL. Reduction of lithium induced interstitial fibrosis on co-administration with amiloride. *Sci Rep*. 2022;12(1):14598. doi:10.1038/s41598-022-18825-1
42. Olivares-Navarrete R, Hyzy SL, Hutton DL, et al. Direct and indirect effects of microstructured titanium substrates on the induction of mesenchymal stem cell differentiation towards the osteoblast lineage. *Biomaterials*. 2010;31(10):2728–2735. doi:10.1016/j.biomaterials.2009.12.029
43. Kaur G, Wang C, Sun J, Wang Q. The synergistic effects of multivalent ligand display and nanotopography on osteogenic differentiation of rat bone marrow stem cells. *Biomaterials*. 2010;31(22):5813–5824. doi:10.1016/j.biomaterials.2010.04.017
44. Hoeflich KP, Luo J, Rubie EA, Tsao MS, Jin O, Woodgett JR. Requirement for glycogen synthase kinase-3beta in cell survival and NF-kappaB activation. *Nature*. 2000;406(6791):86–90. doi:10.1038/35017574
45. Karin M, Clevers H. Reparative inflammation takes charge of tissue regeneration. *Nature*. 2016;529(7586):307–315. doi:10.1038/nature17039
46. Hasan S, Danishuddin M, Adil M, et al. Efficacy of E. officinalis on the cariogenic properties of Streptococcus mutans: a novel and alternative approach to suppress quorum-sensing mechanism. *PLoS One*. 2012;7(7). doi:10.1371/journal.pone.0040319
47. Loesche WJ. Role of Streptococcus mutans in human dental decay. *Microbiol Rev*. 1986;50(4):353–380. doi:10.1128/mr.50.4.353-380.1986
48. Waltimo T, Brunner TJ, Vollenweider M, Stark WJ, Zehnder M. Antimicrobial effect of nanometric bioactive glass 45S5. *J Dent Res*. 2007;86(8):754–757. doi:10.1177/154405910708600813
49. Hu S, Chang J, Liu M, Ning C. Study on antibacterial effect of 45S5 Bioglass. *J Mater Sci Mater Med*. 2009;20(1):281–286. doi:10.1007/s10856-008-3564-5
50. Leppäranta O, Vaahtio M, Peltola T, et al. Antibacterial effect of bioactive glasses on clinically important anaerobic bacteria in vitro. *J Mater Sci Mater Med*. 2008;19(2):547–551. doi:10.1007/s10856-007-3018-5
51. Allan I, Newman H, Wilson M. Antibacterial activity of particulate bioglass against supra- and subgingival bacteria. *Biomaterials*. 2001;22(12):1683–1687. doi:10.1016/s0142-9612(00)00330-6
52. Keikhosravani P, Maleki-Ghaleh H, Kahaie Khosrowshahi A, et al. Bioactivity and antibacterial behaviors of nanostructured lithium-doped hydroxyapatite for bone scaffold application. *Int J Mol Sci*. 2021;22(17):9214. doi:10.3390/ijms22179214
53. Tian Q, Ye J, Yuan W, et al. Highly effective antibacterial activity of lithium-doped magnesium oxide particles synthesized by the microwave-assisted hydrothermal route. *Powder Technology*. 2020;371:130–141. doi:10.1016/j.powtec.2020.05.031
54. Sizar O, Unakal CG. Gram positive bacteria; 2017.
55. Tsao N, Kuo CF, Chiu CC, Lin WC, Huang WH, Chen LY. Protection against Klebsiella pneumoniae using lithium chloride in an intragastric infection model. *Antimicrob Agents Chemother*. 2015;59(3):1525–1533. doi:10.1128/aac.04261-14
56. He L, Zhou J, Chen M, et al. Parenchymal and stromal tissue regeneration of tooth organ by pivotal signals reinstated in decellularized matrix. *Nat Mater*. 2019;18(6):627–637. doi:10.1038/s41563-019-0368-6